

# Reconfigurable structured light generation and its coupling to air-core fiber

Yize Liang<sup>a,b,c</sup>, Hongya Wang<sup>a,b,c</sup>, Xi Zhang<sup>a,b,c</sup>, Jianzhou Ai<sup>a,b,c</sup>, Zelin Ma<sup>d</sup>, Siddharth Ramachandran<sup>d</sup> and Jian Wang<sup>a,b,c,\*</sup>

<sup>a</sup>Huazhong University of Science and Technology, Wuhan National Laboratory for Optoelectronics and School of Optical and Electronic Information, Wuhan, China

<sup>b</sup>Optics Valley Laboratory, Wuhan, China

<sup>c</sup>Shenzhen Institute of Huazhong University of Science and Technology, Shenzhen, China

<sup>d</sup>Boston University, College of Engineering, Boston, Massachusetts, United States

**Abstract.** Recently, structured light beams have attracted substantial attention in many applications, including optical communications, imaging, optical tweezers, and quantum optics. We propose and experimentally demonstrate a reconfigurable structured light beam generator in order to generate diverse structured light beams with adjustable beam types, beam orders, and beam sizes. By controlling the sizes of generated free-space structured light beams, free-space orbital angular momentum (OAM) beams and vector beams are coupled into an air-core fiber. To verify that our structured light generator enables generating structured light with high beam quality, polarization distributions and mode purity of generated OAM beams and vector beams in both free space and air-core fiber are characterized. Such a structured light generator may pave the way for future applications based on higher-order structured light beams.

Keywords: structured light beams; orbital angular momentum; vector beams; air-core fiber.

Received Feb. 15, 2023; revised manuscript received Apr. 6, 2023; accepted for publication May 12, 2023; published online Jun. 12, 2023.

© The Authors. Published by SPIE and CLP under a Creative Commons Attribution 4.0 International License. Distribution or reproduction of this work in whole or in part requires full attribution of the original publication, including its DOI.

[DOI: [10.1117/1.APN.2.3.036015](https://doi.org/10.1117/1.APN.2.3.036015)]

## 1 Introduction

The explosive growth of global data traffic is driving an ever-increasing demand for higher data capacity and more efficient spectral usage in transmission links.<sup>1–3</sup> To address the coming capacity crunch, it is highly desirable not only to make full use of already well-known physical dimensions (e.g., amplitude, phase, frequency/wavelength, polarization, and time) but also to exploit additional degrees of freedom (e.g., spatial structure) of light waves. As a result, space-division multiplexing (SDM) exploiting the transverse spatial structure dimension of light waves has attracted more and more attention.<sup>4,5</sup> SDM technology employing orthogonal higher-order light modes multiplexing can be divided into two different application scenarios, including the free space<sup>6,7</sup> and the optical fiber.<sup>8–11</sup> Among them, the application scenario in optical fiber has the advantages of flexibility and long-distance transmission. Therefore, in recent years,

optical fibers supporting high-order modes have been widely designed, fabricated, and used in SDM applications, such as few-mode fiber,<sup>12,13</sup> traditional multimode fiber,<sup>14</sup> ring-core fiber,<sup>15,16</sup> and air-core fiber.<sup>17,18</sup>

Traditional higher-order modes in fiber, also known as structured light beams due to their different transverse structures,<sup>19–23</sup> can be divided into three types: orbital angular momentum (OAM) beams, linearly polarized (LP) beams, and vector beams. Due to the low loss and flexibility of optical fiber transmission, such diverse structured light beams in optical fibers are widely used in optical communications,<sup>24</sup> optical tweezers,<sup>25</sup> rotating Doppler sensing,<sup>26–29</sup> superresolution imaging,<sup>30,31</sup> and quantum optics.<sup>32,33</sup> Therefore, generating various structured light beams in fiber are required in many applications. There are several approaches to producing structured light beams in fiber, such as mode-selective couplers (MSCs),<sup>34</sup> long-period fiber gratings (LPGs),<sup>35,36</sup> fiber Bragg gratings,<sup>37</sup> and free-space-to-fiber coupling.<sup>14–16</sup> However, for generation of the fourth, fifth, and much higher-order structured light beams in

\*Address all correspondence to Jian Wang, [jwang@hust.edu.cn](mailto:jwang@hust.edu.cn)

optical fiber, the MSCs and LPFGs suffer from a greatly high intensity loss. Thus the method of producing high-order structured light beams in free space and then coupling them into optical fiber is the main way to generate structured light beams with orders higher than fourth in fiber. Remarkably, reconfigurable generation of these structured lights in free space requires a reconfigurable phase-modulation device, such as spatial light modulator (SLM). Different from LP beams and OAM beams, vector beams possess inhomogeneous polarization distributions. Thus approaches for reconfigurable generation of vector beams usually use such steps: splitting a Gaussian beam into two orthogonally polarized beams, modulating them into two OAM beams with opposite topological charges, and then recombining them. There are many experimental setups for generating vector beams based on this principle. In general, these setups can be divided into two categories: one is conventional interferometric setup,<sup>38,39</sup> the other is common-path interferometric loops.<sup>40-43</sup> For conventional interferometric setups, since the two OAM beams propagate along different optical paths, their relative phase difference may alter with time, which will cause the rotation of polarization distributions of a combined vector beam. Such an instability limits applications based on vector beams, including coupling them into optical fiber. In this article, we demonstrate that a common-path interferometric loop will lead to a higher robustness of generated vector beams compared to conventional interferometric setups.

We propose and experimentally demonstrate a reconfigurable structured light beams generator with adjustable beam types, beam orders, and beam sizes. OAM beams, LP beams, and cylindrical vector beams are produced by our scheme in free space. Since beams in the proposed scheme share a common optical path, generated vector beams feature more robustness compared to conventional approach. We measure the Stokes parameters to reconstruct the polarization distributions of beams for verifications. Then OAM beams and vector beams with fifth to seventh mode orders are coupled into a 5-m air-core fiber. At the fiber output, high beam quality and low coupling loss of output higher-order beams are demonstrated, showing that our scheme enables pure high-order structured light generation in optical fiber.

## 2 Results

### 2.1 Scheme of Reconfigurable Structured Light Beams Generator

We propose and experimentally demonstrate a single SLM loop for reconfigurable structured light beams generation. Figure 1(a) illustrates the concept of generating cylindrical vector beams in such a loop. As displayed in Fig. 1(a), the red lines show the track of spatial light, whereas the green and purple arrows represent the transmitting directions of orthogonally polarized beams. In order to produce vector beams, the input Gaussian beam should be 45 deg or -45 deg polarized. Half of the 45 deg polarized beam straightly propagates through the beam splitter (BS), and then it is divided into two orthogonal polarized beams by a polarization beam splitter (PBS). An  $x$ -polarized beam straightly propagates through PBS and transmits in clockwise direction, whereas the  $y$ -polarized beam reflects at PBS and transmits in counterclockwise direction. Gaussian beams are converted into OAM beams by hologram loaded onto SLM, expressed as

$$\text{mod}[(l\varphi + n_g \cdot x - a \cdot r)/2\pi], \quad (1)$$

where the first two components are referred to as a forked phase hologram, which is generally used for generating a pure OAM mode. The  $l\varphi$  term consists of the topological charge  $l$ , and azimuthal angle  $\varphi$  denotes the phase mask of an  $l$ th OAM beam, whereas the  $n_g \cdot x$  term corresponds to the phase mask of an  $x$  direction grating that separates the modulated OAM beam from the unmodulated beam. In addition, the radial grating component  $-a \cdot r$  is applied to form perfect OAM modes with adjustable size<sup>44</sup> (see S3 in the [Supplementary Material](#)). Noting that the phase-only SLM only works on  $x$ -polarized light, a half-wave plate (HWP) is inserted into this loop so as to match the polarization requirement of the SLM and the PBS. At the output of the BS, an  $x$ -polarized OAM beam and a  $y$ -polarized OAM beam are generated with opposite topological charges as a result of different reflected times. Propagating through a quarter-wave plate (QWP),  $x$ - and  $y$ -polarized OAM beams are converted into right-circularly and left-circularly polarized OAM beams. The vector beam is obtained by superposition of these two OAM beams,

$$A_1 \cdot \exp(il\varphi) \begin{bmatrix} 1 \\ \pm i \end{bmatrix} + A_2 \cdot \exp(-il\varphi) \begin{bmatrix} 1 \\ \mp i \end{bmatrix} \cdot \exp(-i\Delta\Phi), \quad (2)$$

where  $\text{abs}(A_1)$  equals to  $\text{abs}(A_2)$  when generating a vector beam, as mentioned above.  $\Delta\Phi$  describes the phase difference of two circularly polarized OAM beams. To further illustrate the relationship between different beam modes, we display the concept of the higher-order Poincaré sphere (HOPS) with  $l = 1$ , as displayed in Fig. 1(b). The poles of the HOPS represent scalar OAM beams (having helical wavefronts) with a uniform circular polarization (right circular at the north pole and left circular at the south pole). The superposition of two poles forms different vector beams with different polarization distributions due to diverse phase difference  $\Delta\Phi$  of two circularly polarized OAM beams, as shown in Fig. 1 (b). In Eq. (2), the type of synthetic vector beams can be changed by adjusting the sign of  $A_1$  and  $A_2$ . Changing the polarization of input Gaussian beam (e.g., +45 deg to -45 deg) means changing the sign of  $A_1$  and  $A_2$ . Rotating the QWP enables the changing of circular polarization state. Therefore, four vector beams on the equator can be generated (see S1 in the [Supplementary Material](#) for details). When generating OAM beams employing this single SLM loop, one can just adjust the incident Gaussian beam to  $x$  or  $y$  polarization. Loading a  $\pm$ OAM superposition phase hologram onto the SLM, LP beams are also generated. In addition, to generate arbitrary vector beams based on this single SLM loop, control of the phase difference of two OAM beams is requested. Many approaches can be utilized to arbitrarily control the phase difference of two OAM beams, including using another SLM or some polarization optics to adjust their phase delay (see S3 in the [Supplementary Material](#) for details). Furthermore, letting the  $x$ -polarized and  $y$ -polarized beams have a slight offset on SLM and then separately modulating them may be another approach to controlling the phase delay of two OAM beams.

A conventional interferometric setup for generation of vector beams obey the rules: splitting a Gaussian beam into two orthogonally polarized beams, modulating them into two OAM beams with opposite topological charges via two phase holograms, and then recombining them. In such a conventional setup,  $\Delta\Phi$  alters, since the two OAM beams propagate along

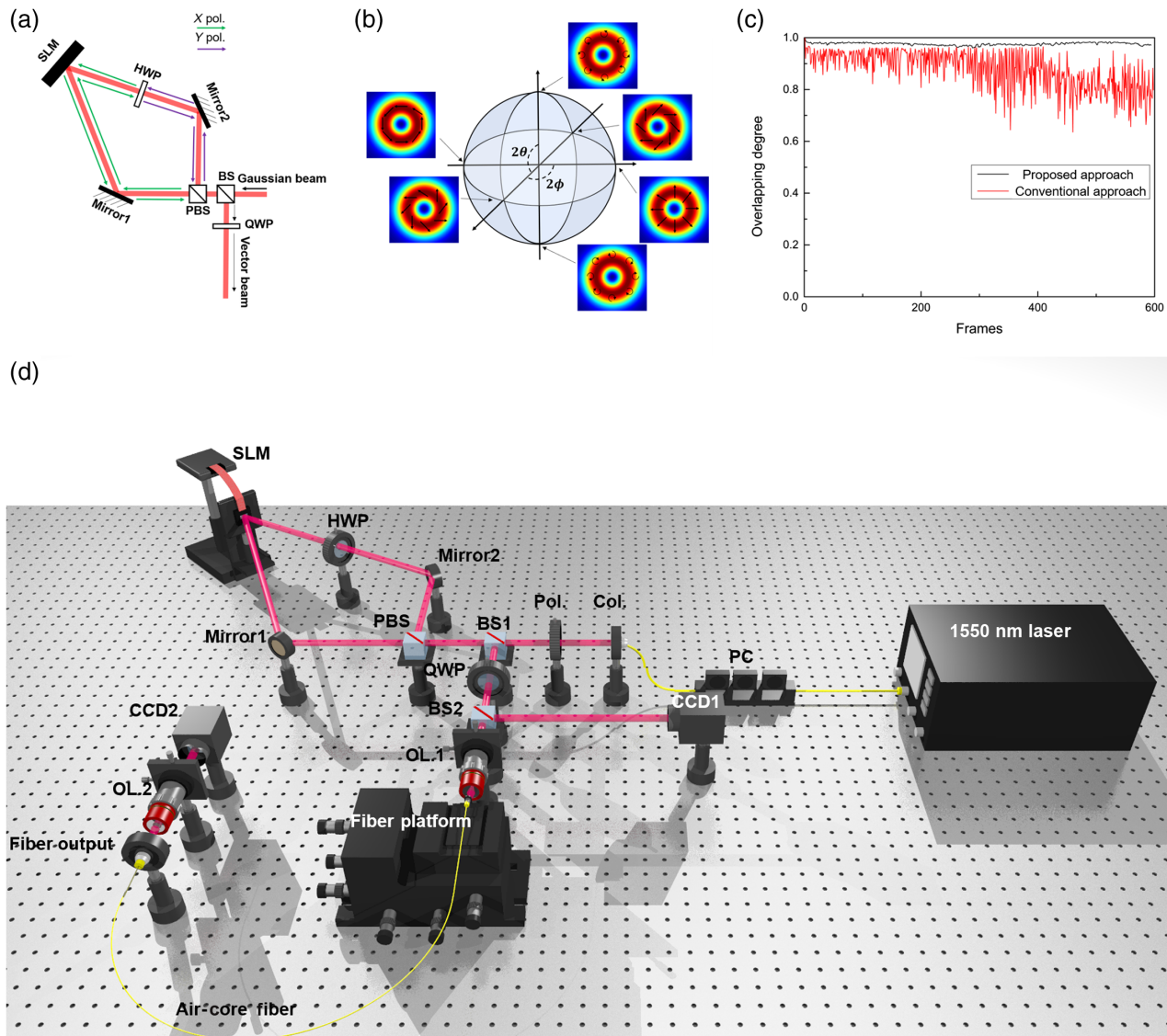


**Fig. 1** (a) Concept of reconfigurable structured light beams generator employing a single SLM loop. (b) HOPS with  $l = 1$ . (c) Overlapping degree between polarization distributions of vector beams in initial frames and vector beams in subsequent frames. (d) Experimental setup of reconfigurable structured light beams generator and fiber-coupling system. PC, polarization controller; Col, collimator; BS, beam splitter; PBS, polarization beam splitter; HWP, half-wave plate; QWP, quarter-wave plate; OL, objective lens; CCD, charge-coupled device (Video 1, mp4, 12.2 MB [URL: <https://doi.org/10.1117/1.APN.2.3.036015.s1>]; Video 2, mp4, 12.1 MB [URL: <https://doi.org/10.1117/1.APN.2.3.036015.s2>]).

different paths. Such a rapid change of  $\Delta\Phi$  may lead to vibration and rotation of the polarization distributions of vector beams, which may be a fundamental disadvantage of conventional approaches. In our approach, the two orthogonal OAM beams share the common optical path so that the polarization distribution of the generated vector beam is robust. An experiment is carried out to demonstrate this point. First, we use two different setups to generate higher-order vector beams. Let the generated vector beams propagate through a polarizer, and the LP-like intensity profiles of vector beams are recorded using a CCD run at 10 frames per second. For a conventional interferometric setup, the lobe jitters and rotates (see Video 1). For common-path interferometric loop in this work, the lobe are stable (Video 2).

Taking the intensity profile of the first frame of recorded video as a reference, the overlapping degree between intensity profiles in other frames and the reference is calculated. As shown in Fig. 1(c), vector beams generated using the proposed approach are stable and robust.

After finishing the construction of reconfigurable structured light beam generator with adjustable beam types, beam orders, and beam sizes, we couple these diverse structured light beams into air-core fiber for testing. The specific experimental setup is shown in Fig. 1(d), with the red line describing the track of spatial light. A polarizer (Pol.) is used to adjust the polarization of the input Gaussian beam. After propagating through the single SLM loop mentioned above, a structured light beam is

generated at the output of the QWP. Then the beam passes through BS2 and is coupled into the air-core fiber by an objective lens (OL1). After the transmission in the air-core fiber, the structured light beam is collimated by OL2. CCD1 and CCD2 capture the intensity profiles of generated structured light beams before and after fiber transmission, respectively. Remarkably, BS2 is used for capturing the free-space structured light, whereas BS1 applied due to the SLM is a polarization-sensitive device. Such two BSs lead to a 9-dB loss, which is a disadvantage for power-limited structured light beam applications. Thus one can further improve the transmission efficiency of this setup by removing the two BSs (see S7 in the [Supplementary Material](#) for details).

## 2.2 Polarization Reconstruction of Structured Light Beams

To verify the generated structured light beams, an approach is developed to measure the polarization distributions of structured light beams, especially for vector beams. Figs. 2(a)–2(g) illustrate the polarization reconstruction process of vector beam with mode order  $l = 1$ , whereas Figs. 2(h)–2(n) correspond to mode order  $l = 10$ .

Noting that the polarization of the uniform polarized beam can be described by Stokes parameters, we achieve the

polarization measurement of the vector beams by calculating the Stokes parameters of each point at the transverse plane. Stokes parameters are known to be calculated as

$$\begin{cases} S_0 = I_X + I_Y \\ S_1 = I_X - I_Y \\ S_2 = I_{+45} - I_{-45} \\ S_3 = I_R - I_L \end{cases}, \quad (3)$$

where  $S_0 - S_3$  represent four Stokes parameters.  $I_X$ ,  $I_Y$ ,  $I_{+45}$ , and  $I_{-45}$  correspond to the intensity of light passing through a polarizer whose direction is adjusted to  $x$ ,  $y$ ,  $+45$  deg, and  $-45$  deg, respectively.  $I_R$  corresponds to the intensity of light passing through a  $+45$  deg directional QWP and an  $x$ -directional polarizer, representing the right-circularly polarized component.  $I_L$  corresponds to the intensity of light passing through a  $+45$  deg directional QWP and a  $y$  directional polarizer, representing the left-circularly polarized component. For cylindrical vector beams, by recording six different intensity profiles, one can easily calculate the Stokes parameters of each point at the beam transverse plane. Thus the function of the light field can be calculated employing the known Stokes parameters of each point, which can be written as

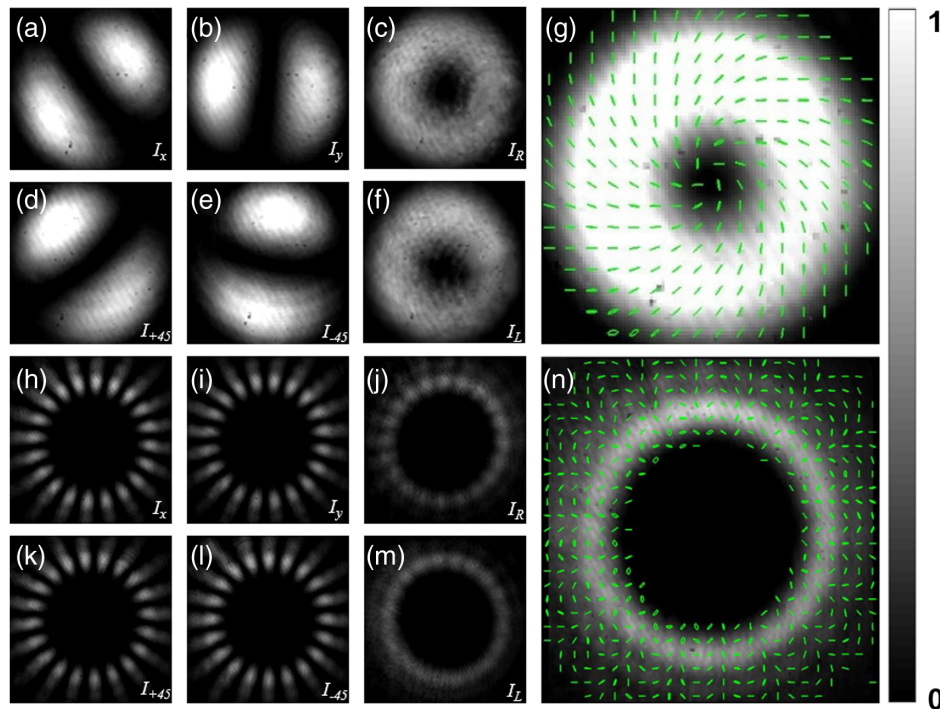


**Fig. 2** Polarization reconstruction of cylindrical vector beams. Measured intensity profiles of a vector beam with mode order  $l = 1$  after propagating through (a) an  $x$ -polarized polarizer; (b) a  $y$ -polarized polarizer; (c) a  $+45$  deg directional QWP and an  $x$ -polarized polarizer; (d) a  $+45$  deg polarizer; (e) a  $-45$  deg polarizer; (f) a  $+45$  deg directional QWP and a  $y$ -polarized polarizer; (g) intensity profile and polarization distribution of the vector beam with mode order  $l = 1$ . Measured intensity profiles of a vector beam with mode order  $l = 10$  after propagating through (h) an  $x$ -polarized polarizer; (i) a  $y$ -polarized polarizer; (j) a  $+45$  deg directional QWP and an  $x$ -polarized polarizer; (k) a  $+45$  deg polarizer; (l) a  $-45$  deg polarizer; (m) a  $+45$  deg directional QWP and a  $y$ -polarized polarizer; (n) intensity profile and polarization distribution of the vector beam with mode order  $l = 10$ .

$$\begin{cases} E_X = \sqrt{(1 + S_1/S_0)/2} \cdot \cos \varphi \\ E_Y = \sqrt{(1 - S_3/S_2)/2} \cdot \cos[\varphi + \tan^{-1}(S_3/S_2)] \end{cases} \quad (4)$$

where  $E_X$  and  $E_Y$  describe the simple harmonic vibration functions of light in two orthogonal directions.  $\varphi$  represents the transmission and vibration phase of light, usually described as  $\varphi = k \cdot z - \omega \cdot t + \varphi_0$ . Thus the trajectory of the beam vector determined by  $E_X$  and  $E_Y$  can be calculated by taking the value of  $\varphi$  from 0 to  $2\pi$  in the parameter equation system about  $\varphi$ .

By capturing the intensity profiles of  $I_X$ ,  $I_Y$ ,  $I_{+45}$ ,  $I_{-45}$ ,  $I_R$ , and  $I_L$ , as shown in Figs. 2(a)–2(f) or Figs. 2(h)–2(m), respectively, we calculate the Stokes parameters and then give the polarization of each point. It is worth mentioning that all the intensity profiles are divided into many small matrices in order to facilitate the final marking of the polarization in the reconstruction figure, such as in Figs. 2(g) and 2(n).

### 2.3 Reconfigurable Structured Light Beams Generated in Free Space

Loading the seventh order hologram ( $l = 7$ ) onto the SLM, by adjusting the polarization devices in the experimental setup, we obtain diverse structured light beams, such as  $x$ -polarized OAM beams,  $x$ -polarized LP beams, circularly polarized OAM beams, and vector beams in free space. CCD1 in Fig. 1(d) is used to capture the intensity profiles of the generated beams.

Figure 3 displays all types of structured light beams with the seventh order generated in our setup. We record the intensity profiles and reconstruct the polarization distributions of  $x$ -polarized OAM beams with opposite topological charges (i.e.,  $+7$  and  $-7$ ), as shown in Figs. 3(a) and 3(b). Moreover, we record the intensity profiles of OAM beams interfering with Gaussian beams in order to verify the topological charge of OAM beams, as inserted into the right side of Fig. 3(b). The upper one denotes the interference intensity profile of OAM mode in Fig. 3(a),

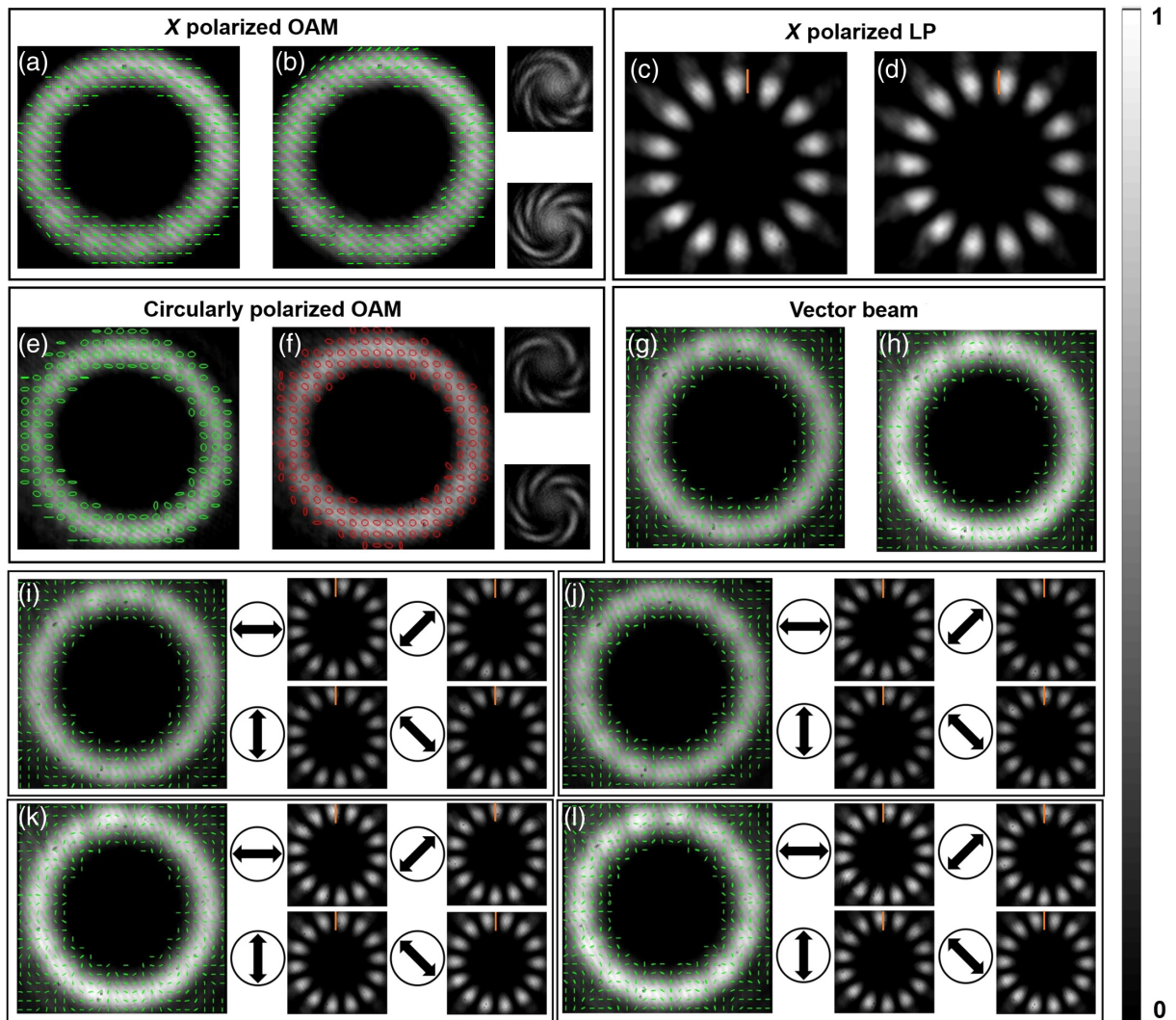


**Fig. 3** Intensity profiles and polarization distributions of diverse seventh-order structured light beams generated in free space. (a), (b)  $x$ -polarized OAM beams, insets are interference intensity profiles of them. (c), (d)  $x$ -polarized LP beams. (e), (f) Circularly polarized OAM beams, insets are interference intensity profiles of them. (g), (h) Vector beams. (i)–(l) Four different vector beams; insets are intensity profiles of vector beams passing through different directional polarizers.

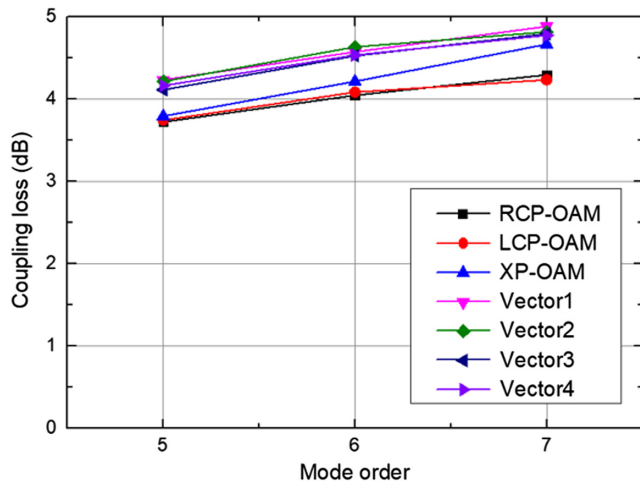


**Fig. 4** Coupling losses of the fourth to seventh OAM and vector beams. RCP, right circular polarization; LCP, left circular polarization; and XP, x polarization.

whereas the bottom one corresponds to the interference intensity profile of OAM mode in Fig. 3(b). Figures 3(c) and 3(d) illustrate the obtained  $x$ -polarized LP beams, with orange vertical lines marked to distinguish different LP modes. Circularly polarized OAM beams with opposite topological charges, mentioned as poles on HOPS, are shown in Figs. 3(e) and 3(f). For circularly polarized OAM beams, green lines indicate the right circular polarizations, whereas red lines indicate the left circular polarizations. Similarly, interference intensity profiles are also inserted into the right side of Fig. 3(f). The upper one denotes the interference intensity profile of the OAM mode in Fig. 3(e), whereas the bottom one corresponds to the interference intensity profile of the OAM mode in Fig. 3(f).

Figures 3(g) and 3(h) display the intensity profiles and polarization distributions of two different seventh-order vector beams.

Four vector beams with different polarization distributions are generated in this experimental setup by adjusting the polarization devices, as illustrated in Figs. 3(i)–3(l). They possess a measured average polarization purity of 94.0% (94.2%, 93.3%, 94.3%, and 94.3%) for four different vector beams, respectively (see S9 in the [Supplementary Material](#) for details).<sup>45,46</sup> Intensity profiles of four different vector beams passing through different directional polarizers are also displayed, as shown in Figs. 3(i)–3(l). Orange vertical lines are marked to distinguish these LP-like intensity profiles. With the rotation of polarizer (from horizontal to 45 deg, vertical,  $-45$  deg), lobes in Figs. 3(i) and 3(k) rotate clockwise, whereas lobes in Figs. 3(j) and 3(l) rotate counterclockwise.

#### 2.4 Diverse Structured Light Beams after Transmission through Air-Core Fiber

Noting that the air-core fiber is a strongly guiding fiber (LP beams are not supported in air-core fiber), only free-space vector beams and OAM beams are coupled into the air-core fiber. By adjusting the divergence of such free-space structured light, the size match between focused structured light and ring-shaped fiber core can be accomplished. Hence, fifth to seventh OAM beams and vector beams can be coupled into the air-core fiber with losses  $<5$  dB, as displayed in Fig. 4. Vector 1 to vector 4 represent four different vector beams generated in the interferometric loop (see S1 in the [Supplementary Material](#) for details).

The quality of output beam is another way to prove that accurate coupling of higher-order modes is accomplished in our scheme. We accordingly capture the intensity profiles of OAM beams and vector beams output from the 5-m air-core fiber using CCD2, as shown in Fig. 5. It can be seen from Figs. 5(a)–5(d) that  $x$ -polarized and circularly polarized

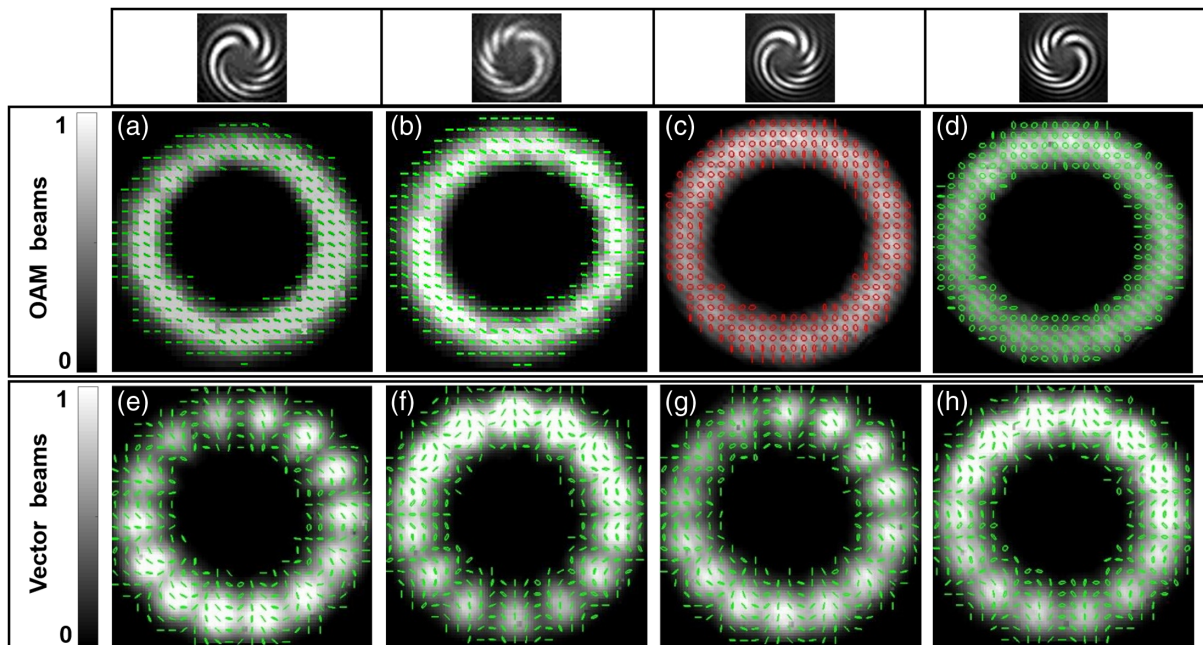


**Fig. 5** Diverse seventh-order structured light beams after 5-m air-core fiber transmission, insets above figures (a)–(d) are their interference intensity profiles, respectively. (a), (b)  $x$ -polarized OAM beams; (c), (d) circularly polarized OAM beams; and (e)–(h) vector beams.

OAM beams still possess the same uniform polarization distributions after transmission of air-core fiber. In addition, all the interference intensity profiles of OAM beams and fundamental Gaussian beams are recorded, demonstrating the high purity of output OAM beams (see S8 in the [Supplementary Material](#)). For output vector beams, they still remain periodic polarization distributions, as shown in Figs. 5(e)–5(h). Polarization purity of the fiber-guided vector beams are also calculated, possessing an average polarization purity of 91.6% (92.9%, 90.8%, 91.1%, and 91.5%) for four different vector modes, respectively (see S9 in the [Supplementary Material](#) for details).

### 3 Conclusion

In summary, we propose and experimentally demonstrate a reconfigurable structured light beam generator. Diverse structured light beams, such as OAM beams, LP beams, and vector beams with controllable mode orders and sizes are generated in free space. For ring-shaped uniformly polarized OAM beams and ring-shaped nonuniformly polarized cylindrical vector beams, we measure the Stokes parameters of each point at the transverse plane to reconstruct the polarization distributions for distinguishing these two beams. In order to produce and transmit higher-order structured light beams in optical fiber, we couple the generated fifth- to seventh-order OAM beams and vector beams into 5-m air-core fiber. Low coupling loss (<5 dB for all supported modes) and high purity of structured light beams are obtained, further proving that we have produced and transmitted stable structured light beams in fiber.

There are already some other devices to generate structured light beams, including digital micromirror devices,<sup>47</sup> metasurfaces,<sup>48</sup> Q-plates,<sup>49</sup> and J-plates.<sup>50</sup> Digital micromirror devices are another kind of free-space device to tailor the spatial transverse structure of light beams, which might be used to replace the SLM in the interferometric loop. Although metasurfaces, Q-plates, and J-plates can also generate structured light with high robustness, they are usually not reconfigurable. Hence, the single-SLM Sagnac loop approach in this study takes advantage of both high robustness and reconfiguration. Such reconfigurable structured light beams generator may act as a useful scheme for various free-space and fiber-optic applications based on structured light beams, such as SDM communications, optical tweezers, optical sensing, superresolution imaging, and quantum optics.

### Data Availability Statement

The data that support the findings of this study are available from the corresponding author upon reasonable request.

### Acknowledgments

This work was supported by the National Natural Science Foundation of China (Grant Nos. 62125503 and 62261160388), the Key R&D Program of Hubei Province of China (Grant Nos. 2020BAB001 and 2021BAA024), the Key R&D Program of Guangdong Province (Grant No. 2018B030325002), the Shenzhen Science and Technology Program (Grant No. JCYJ20200109114018750), the Open Projects Foundation of State Key Laboratory of Optical Fiber and Cable Manufacture Technology (Grant No. SKLD2201), and the Innovation Project of Optics Valley Laboratory (Grant No. OVL2021BG004). The authors declare no conflicts of interest.

### References

1. R. Essiambre et al., “Capacity limits of optical fiber networks,” *J. Lightwave Technol.* **28**(4), 662–701 (2010).
2. R. Essiambre and R. W. Tkach, “Capacity trends and limits of optical communication networks,” *Proc. IEEE* **100**(5), 1035–1055 (2012).
3. Y. Liang et al., “Experimental demonstration of visualized multi-core fiber coupling alignment system for inter-core cross talk measurement,” *Opt. Lett.* **47**(12), 3071–3074 (2022).
4. G. Li et al., “Space-division multiplexing: the next frontier in optical communication,” *Adv. Opt. Photonics* **6**(4), 413–487 (2014).
5. J. Wang, “Advances in communications using optical vortices,” *Photonics Res.* **4**(5), B14–B28 (2016).
6. J. Wang et al., “Terabit free-space data transmission employing orbital angular momentum multiplexing,” *Nat. Photonics* **6**(7), 488–496 (2012).
7. Y. Liang et al., “Adaptive turbulence compensation and fast auto-alignment link for free-space optical communications,” *Opt. Express* **29**(24), 40514–40523 (2021).
8. N. Bozinovic et al., “Terabit-scale orbital angular momentum mode division multiplexing in fibers,” *Science* **340**(6140), 1545–1548 (2013).
9. G. Zhu et al., “Scalable mode division multiplexed transmission over a 10-km ring-core fiber using high-order orbital angular momentum modes,” *Opt. Express* **26**(2), 594–604 (2018).
10. J. Liu et al., “Direct fiber vector eigenmode multiplexing transmission seeded by integrated optical vortex emitters,” *Light Sci. Appl.* **7**(3), 17148 (2018).
11. J. Zhang et al., “Mode-division multiplexed transmission of wavelength-division multiplexing signals over a 100-km single-span orbital angular momentum fiber,” *Photonics Res.* **8**(7), 1236–1242 (2020).
12. H. Huang et al., “Mode division multiplexing using an orbital angular momentum mode sorter and MIMO-DSP over a graded-index few-mode optical fibre,” *Sci. Rep.* **5**(1), 1–7 (2015).
13. Y. Liang et al., “2.6-km all-fiber orbital angular momentum (OAM) multiplexing link for data center networks (DCNs) using mode select coupler and commercial SFP+ transceivers,” presented at the *CLEO: Sci. and Innov.* (2018).
14. A. Wang et al., “Directly using 8.8-km conventional multi-mode fiber for 6-mode orbital angular momentum multiplexing transmission,” *Opt. Express* **26**(8), 10038–10047 (2018).
15. J. Zhang et al., “Orbital-angular-momentum mode-group multiplexed transmission over a graded-index ring-core fiber based on receive diversity and maximal ratio combining,” *Opt. Express* **26**(4), 4243–4257 (2018).
16. H. Wang et al., “Low-loss orbital angular momentum ring-core fiber: design, fabrication and characterization,” *J. Lightwave Technol.* **38**(22), 6327–6333 (2020).
17. P. Gregg, P. Kristensen, and S. Ramachandran, “Conservation of orbital angular momentum in air-core optical fibers,” *Optica* **2**(3), 267–270 (2015).
18. K. Ingerslev et al., “12 Mode, MIMO-free OAM transmission,” presented at *2017 Opt. Fiber Commun. Conference and Exhibit. (OFC)* (2017).
19. Q. Zhan, “Cylindrical vector beams: from mathematical concepts to applications,” *Adv. Opt. Photonics* **1**(1), 1–57 (2009).
20. A. Forbes, M. de Oliveira, and M. R. Dennis, “Structured light,” *Nat. Photonics* **15**(4), 253–262 (2021).
21. A. Rubano et al., “Q-plate technology: a progress review,” *JOSA B* **36**(5), D70–D87 (2019).
22. M. Piccardo et al., “Roadmap on multimode light shaping,” *J. Opt.* **24**(1), 13001 (2021).
23. H. Rubinsztein-Dunlop et al., “Roadmap on structured light,” *J. Opt.* **19**(1), 13001 (2016).
24. Z. Xie et al., “Ultra-broadband on-chip twisted light emitter for optical communications,” *Light Sci. Appl.* **7**(4), 18001 (2018).

25. M. Padgett and R. Bowman, "Tweezers with a twist," *Nat. Photonics* **5**(6), 343–348 (2011).
26. M. P. Lavery et al., "Detection of a spinning object using light's orbital angular momentum," *Science* **341**(6145), 537–540 (2013).
27. L. Fang, M. J. Padgett, and J. Wang, "Sharing a common origin between the rotational and linear Doppler effects," *Laser Photonics Rev.* **11**(6), 1700183 (2017).
28. Z. Wan et al., "Flexible and robust detection of a remotely rotating target using fiber-guided orbital angular momentum superposed modes," presented at *2020 Conf. Lasers and Electro-Optics (CLEO)* (2020).
29. Z. Wan et al., "Remote measurement of the angular velocity vector based on vectorial Doppler effect using air-core optical fiber," *Research (Wash D C)* **2022**, 9839502 (2022).
30. L. Yan, P. Kristensen, and S. Ramachandran, "Vortex fibers for STED microscopy," *APL Photonics* **4**(2), 022903 (2019).
31. J. Wang and Y. Liang, "Generation and detection of structured light: a review," *Front. Phys.* **9**, 263 (2021).
32. Y. Zhang et al., "Simultaneous entanglement swapping of multiple orbital angular momentum states of light," *Nat. Commun.* **8**(1), 1–7 (2017).
33. J. Liu et al., "Multidimensional entanglement transport through single-mode fiber," *Sci. Adv.* **6**(4), y837 (2020).
34. T. Wang et al., "Generation of femtosecond optical vortex beams in all-fiber mode-locked fiber laser using mode selective coupler," *J. Lightwave Technol.* **35**(11), 2161–2166 (2017).
35. Y. Zhao et al., "All-fiber mode converter based on long-period fiber gratings written in few-mode fiber," *Opt. Lett.* **42**(22), 4708–4711 (2017).
36. Y. Han et al., "Controllable all-fiber generation/conversion of circularly polarized orbital angular momentum beams using long period fiber gratings," *Nanophotonics* **7**(1), 287–293 (2018).
37. L. Wang et al., "Characterization of OAM fibers using fiber Bragg gratings," *Opt. Express* **22**(13), 15653–15661 (2014).
38. C. Maurer et al., "Tailoring of arbitrary optical vector beams," *New J. Phys.* **9**(3), 78 (2007).
39. H. Chen et al., "Generation of vector beam with space-variant distribution of both polarization and phase," *Opt. Lett.* **36**(16), 3179–3181 (2011).
40. S. Liu et al., "Generation of arbitrary spatially variant polarization beams with a trapezoid Sagnac interferometer," *Opt. Express* **20**(19), 21715–21721 (2012).
41. S. Li et al., "An efficient and robust scheme for controlling the states of polarization in a Sagnac interferometric configuration," *Europhys. Lett.* **105**(6), 64006 (2014).
42. P. Li et al., "Generation of perfect vectorial vortex beams," *Opt. Lett.* **41**(10), 2205–2208 (2016).
43. C. Yang et al., "Nonlinear frequency conversion and manipulation of vector beams in a Sagnac loop," *Opt. Lett.* **44**(2), 219–222 (2019).
44. P. Vaity and L. Rusch, "Perfect vortex beam: Fourier transformation of a Bessel beam," *Opt. Lett.* **40**(4), 597–600 (2015).
45. Z. E. Bomzon, V. Kleiner, and E. Hasman, "Formation of radially and azimuthally polarized light using space-variant subwavelength metal stripe gratings," *Appl. Phys. Lett.* **79**(11), 1587–1589 (2001).
46. G. Machavariani et al., "Birefringence-induced bifocusing for selection of radially or azimuthally polarized laser modes," *Appl. Opt.* **46**(16), 3304–3310 (2007).
47. K. J. Mitchell et al., "High-speed spatial control of the intensity, phase and polarisation of vector beams using a digital micromirror device," *Opt. Express* **24**(25), 29269–29282 (2016).
48. X. Yi et al., "Generation of cylindrical vector vortex beams by two cascaded metasurfaces," *Opt. Express* **22**(14), 17207–17215 (2014).
49. W. Ji et al., "Meta-q-plate for complex beam shaping," *Sci. Rep.* **6**(1), 25528 (2016).
50. Y. Huang et al., "Versatile total angular momentum generation using cascaded J-plates," *Opt. Express* **27**(5), 7469–7484 (2019).

**Yize Liang** received his BS degree from Huazhong University of Science and Technology in 2018. Currently, he is pursuing his PhD at Wuhan National Laboratory for Optoelectronics and School of Optical and Electronic Information at Huazhong University of Science and Technology. His research interests include structured light and multimode fibers.

**Hongya Wang** received his BS degree and his PhD from Huazhong University of Science and Technology in 2016 and 2023, respectively. He is currently an R&D engineer at the ZTE Corp. His research interests include intelligent optical transmission system and mode-division multiplexing over fibers.

**Xi Zhang** received his BE degree from Nanjing University of Technology, Nanjing, China. He is currently pursuing his PhD at Wuhan National Laboratory for Optoelectronics and School of Optical and Electronic Information of Huazhong University of Science and Technology. His research interests include specialty passive optical fibers, active optical fibers, and high-speed optical communications.

**Jianzhou Ai** received his BS degree and master's degree from Huazhong University of Science and Technology in 2016 and 2019, respectively. He is currently an R&D engineer at Huawei Technologies Corp.

**Zelin Ma** received his BS degree from Sun Yat-sen University in 2015. Currently, he is pursuing his PhD in electrical engineering at High Dimensional Photonics Lab at Boston University. His research interests include light with orbital angular momentum in optical fibers for telecommunications.

**Siddharth Ramachandran** started his career at Bell Labs, and after a decade in industrial research labs, returned to academia, where he is currently a Distinguished Professor of engineering at Boston University. His work on the understanding and development of lightwave devices comprising spatial, vectorial and topological complexity have been applied in the fields of quantum computing, optical networks, brain imaging, as well as laser-based defense systems. For his contributions, he has been named a Distinguished Member of Technical Staff at OFS (2003), a fellow of Optica (2010), IEEE (2019), SPIE (2019), and APS (2022), an IEEE Distinguished Lecturer (2013 to 2015), a Distinguished Visiting Fellow of UK Royal Society of Engineering (2016), and a Vannevar Bush Faculty Fellow (2019). He serves the optics and photonics community in several capacities, including, currently, as a deputy editor for Optica.

**Jian Wang** received his PhD in physical electronics from Wuhan National Laboratory for Optoelectronics, Huazhong University of Science and Technology, China, in 2008. He worked as a postdoctoral research associate at the Optical Communications Laboratory, University of Southern California, United States, from 2009 to 2011. Currently, he is working as a professor at Wuhan National Laboratory for Optoelectronics, Huazhong University of Science and Technology, China. He is a vice director of Wuhan National Laboratory for Optoelectronics, Huazhong University of Science and Technology, China. He was elected as an OPTICA fellow (formerly OSA fellow) in 2020 and an SPIE fellow in 2022. He leads the Multi-dimensional Photonics Laboratory. His research interests include optical communications, optical signal processing, silicon photonics, photonic integration, orbital angular momentum, and structured light.